What Lies Discarded:
Search for new physics from Long-Lived Particles in the ATLAS detector

The University of Texas at Austin

Vijay Venu Thiyagarajan

Supervised by Prof. Tim Andeen

May 4, 2020

Abstract

At the record-breaking energies of today's particle accelerators many types of new particles are expected to be observable. However, since 2012, no new particles have been discovered. We suspect the particles we are looking for could be long-lived particles (LLPs), for which the detectors were not designed for. The signals from proton-proton collisions received by the calorimeters in the ATLAS detector at the Large Hadron Collider at CERN are converted into meaningful information about the particles through a process called reconstruction. The reconstruction at ATLAS is done by assuming most of the points in space where a parent particle decays into its daughter particles, called decay vertices, are within 15 centimetes of the center of the 25 meters wide detector. However, LLPs, as they are long-lived, have displaced decay vertices, which leads to LLP signals either being reconstructed inaccurately or discarded as uninteresting data. To reconstruct those LLP decay vertices, an algorithm was designed which used cell-level information of the calorimeter as its input. The algorithm was tested on simulations of Higgs bosons decaying into two photons at various positions in the detector. The distance between the decay vertex from the simulation (truth) and the decay vertex from the algorithm (candidate) was compared to the distance between the truth vertex and the decay vertex from the standard reconstruction (primary). If the candidate vertex was found 50-75 cm from the origin and within 25 cm from the beam pipe, or if it was found in the outer regions of the Inner Detector, i.e, the candidate vertex had 50 cm $<\mid z \mid <$ 115 cm, or 75 cm $<\mid r \mid = \sqrt{x^2 + y^2} <$ 115 cm, then there would be an 80 percent chance of $d(\text{candidate}, \text{truth}) < d(\text{primary}, \text{truth})$. This will translate to higher chances of observing statistically significant signals of LLPs when the sample size is increased many-fold.

Acknowledgements

My biggest thanks to my parents, for making it possible for me to leave the country at 18 and pursue my education in Texas. Special thanks to all my instructors and professors, and to Tim, who all have supported me throughout and enriched my life in more ways than just the dispersion of knowledge could. Nothing would be possible or worth it were it not for all the friends I made during my time here, and all my friends from India, thank you.

Contents

Chapter 1

Introduction

1.1 Background

One of the primary goals of particle physics experiments is to observe new physics, which would appear as new, hypothesized particles. The process of observing new particles is complicated by the small signal size, which results in the application of sophisticated statistical methods. The Higgs boson was the latest major discovery among the particle physics community; it has been eight years since and no new physics has been observed at the record-breaking energy levels of leading experiments (like ATLAS), despite several predictions of particles beyond the Standard Model of Physics.

The ATLAS detector is a 44 m long and 25 m wide cylindrical machine composed of giant magnets and calorimeters designed for detecting quarks, leptons, and bosons (see Fig. 1.1). Clouds of protons are accelerated to very high energies (TeV) in the Large Hadron Collider at CERN, a 27km long circular evacuated beam pipe in Geneva, Switzerland, and are made to collide at the center of the ATLAS detector. The colliding clouds of protons results in a shower of all types of particles coming from the center of the detector, whose signals get picked up by the detector, which is followed by particle physicists analyzing the signals, by comparing with simulations, to deduce which particles led to which signals. This is the brief story behind how the scientists at CERN discovered the Higgs Boson in 2012. However, a single event (proton-proton collision) produces about 25 megabytes of data; a single second produces a petabyte (1,000,000,000 megabytes) of raw data. This data challenge leaves scientists with no other option but to throw away

most of the data in order to have manageable amounts of data. This filtering is done by an automated trigger system. From the 1.7 billion collisions that occur each second in the centre of the detector, the trigger system discards all but a 1000 events. Data can be discarded for several reasons - uninteresting or already seen physics, indiscernible signals, etc.

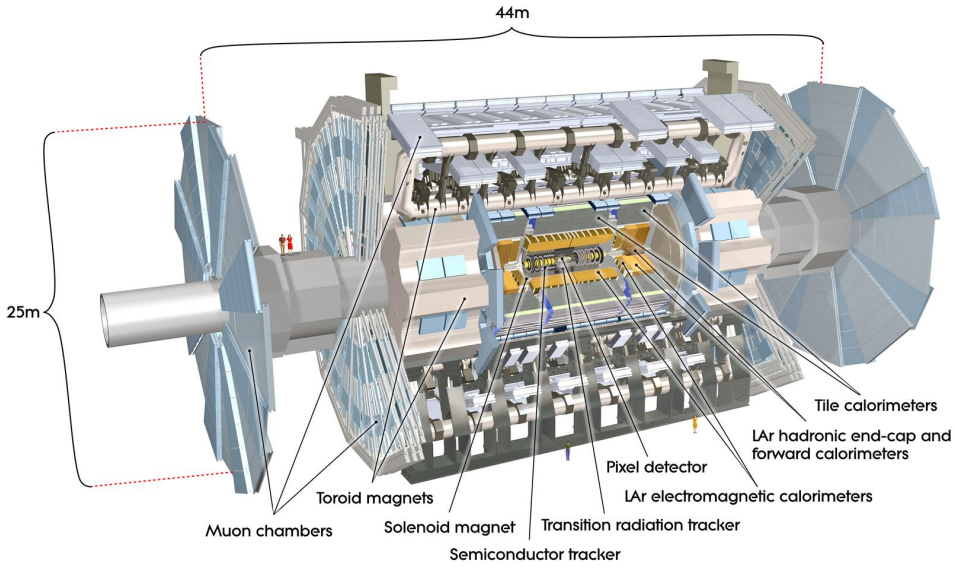

Figure 1.1: Computer generated image of the ATLAS detector. © CERN.

The detector consists of several concentric layers built around the collision point. The major components are the Inner Detector, the Calorimeters, the Muon Spectrometer and the Magnet System. The Inner Detector measures the direction, momentum, and charge of electrically-charged particles, the Muon Spectrometer identifies and measures the momenta of muons, and the Magnet System bends the trajectories of each charged particle to allow the measurement of its momentum. Relevant for this study are the calorimeters, specifically the electromagnetic (EM) calorimeter, which measures the energy electrons and photons lose as it passes the detector. They are designed to stop the particles passing through and force them to deposit all their energy in the detector. The EM calorimeter is divided into four layers, each layer is divided into cells, and the resolution (size) of the cells varies

among the layers (see Fig. 1.2) [14].

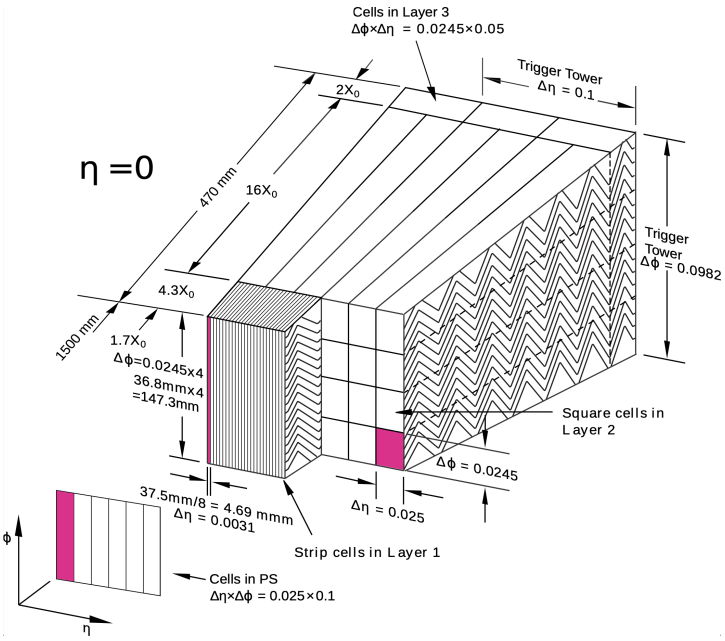

Figure 1.2: Cell resolution of the four layers of the LAr EM calorimeter.

Proton-proton collisions result in complicated and unpredictable decay chains. For example, the Higgs Boson from a proton-proton collision has been observed to decay into a pair of Z bosons leading to two pairs of charged leptons, 2 W bosons leading to 2 charged leptons and 2 neutrinos, or a pair of photons, among other decay modes. The scientists are given observables pertaining to the final state particles (the particles at the ends of the decay chains), such as energy, momentum, trajectory, and position in the detector, and they reconstruct the entire decay chain along with directly unobservable quantities such as mass of the particles, location of the decay vertices, charge, etc.

1.2 Motivation

The assumption is, among the recorded physics data, the final decay vertices of all observable and useful events are within about 15cm of the origin of the 25 meters wide detector, and thus the standard ATLAS reconstruction

of events is performed with this assumption [3]. This means that events in which if final decay vertices are significantly farther away from the origin, say 75cm, could be discarded by the trigger system as the erroneous standard reconstruction could produce meaningless or useless information, and thus new physics could be lost.

Long-lived particles (LLPs) are a subset of the particle-zoo which includes particles that decay after significantly longer period of time than a tenth of a nanosecond. These LLPs, because they exist for longer periods of time than typical particles observed at ATLAS (which are assumed to decay within about 15cm of the origin), decay farther away from the origin. If a particle with a lifetime of a nanosecond was produced at the origin, it could decay into its daughter particles at about 1 light-nanosecond away from the origin, which is about 30 centimeters. LLPs are a common prediction of a range of theories that address un-solved fundamental physics problems such as dark matter, baryogenesis, neutrino masses, and of course, physics beyond the Standard Model (BSM). For the purpose of this report, we deal with events with LLPs which decay within a radial distance of about a meter from the beam pipe, which translates to maximum lifetimes of about 3 nanoseconds; this ensures the parent particle decays before it reaches the EM calorimeter. See Discussion for possible BSM and other particles with lifetimes less than 3 nanoseconds.

The motivation is to design an algorithm that would take the cell-level information from the EM calorimeter of these LLP events and reconstruct the location of the displaced decay vertex. Detector readouts of 200,000 events were simulated, where a Higgs boson was required to decay into two photons at locations far away from the origin. From the cell-level information of the EM calorimeter, i.e, the energy recorded by and the position of every cell of all four layers of the EM calorimeter, it would be possible to identify the cells which correspond to the two photons. Since photons travel in straight lines in the detector (as opposed to curved trajectories of charged particles), a line could be fit through the cells that got 'hit' by the photons. Once both lines are determined, the point of intersection should give the decay vertex from which these photons emerged. We call this point of intersection the candidate vertex.

By comparing the candidate vertices to the truth (from the simulation) vertices and the primary (from the standard reconstruction) vertices, an

idea can be formed of how effective this method of reconstructing photon tracks and decay vertices is in representing accurately these LLP events. Additional selections can be made on the sample of events to search for regions of the parameter space where the algorithm performs significantly better.

Chapter 2

Methods

2.1 Simulation

Detector readouts of events were simulated with a Geant4 [6] particle gun to generate the desired LLP signals. Events were reconstructed using the standard ATLAS software [1] [2] [4] [5]. Monte Carlo simulations of proton-proton collisions using Pythia8(v8.210) [13] and EvtGen(v1.2.0) were performed to generate realistic background noise.[1] [11]. Analysis was done with ROOT [8] and Python3. The particle gun 'shot' Higgs bosons from a variety of positions within 115cm in the radial direction, with a variety of momenta (Higgs transverse momentum ranges from 0 to 500 GeV, flatly distributed), and it was required the Higgs decay into two photons immediately. The position where the Higgs boson was placed in an event is the Truth decay vertex of that event, and in a sense 'the correct answer'. The closer the reconstructed vertex is to the truth vertex, the more 'correct' the reconstruction. Among the 200,000 events simulated, only 101,964 will be detectable by the detector, i.e, the photons have transverse momentum $P_t > 25$ MeV/c, and have truth and candidate vertices below the EM calorimeter (radial distance $r < 115$ cm). We called these collection of events the master sample.

As can be seen in Fig. 2.1, while the truth vertices are distributed throughout the volume of the cylinder, the vertices reconstructed from the standard ATLAS reconstruction, called Primary vertices, are all within 15cm

[1] The events have High-pT inelastic minimum bias events for pile-up, with the A3 NNPDF23LO tune.

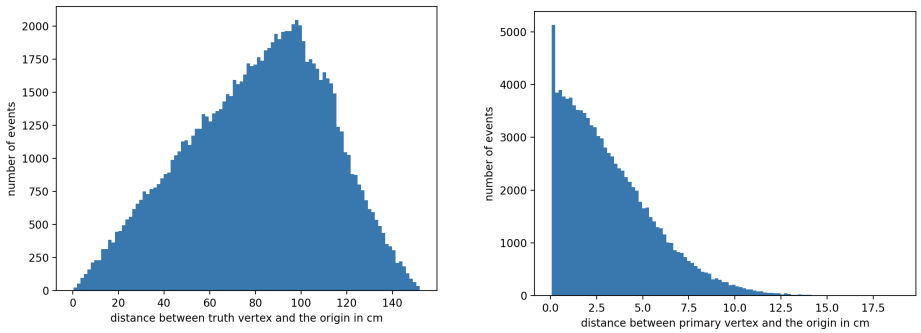

Figure 2.1: Distribution of the truth and primary vertices in the master sample. Note all the primary vertices are within 15cm from the origin. Sample size = 101,964.

of the origin.

For every event from the master sample, the cell-level information was obtained. It consists of the energy deposition E, pseudorapidity $\eta = -\ln(\tan\theta/2)$, azimuthal angle ϕ, the z-coordinate, and the radial distance $r = \sqrt{x^2 + y^2}$ value for each cell of each layer. θ is inclination angle, i.e, the angle with respect to the z-axis. Layer 0 of EM calorimeter has 10,880 cells, layer 1 has 90,784 cells, layer 2 has 54,952 cells, and layer 3 has 25,852 cells, giving a total of 182,468 cells for which all these quantities were obtained.

2.2 Algorithm

The algorithm takes the above cell-level information for an event and returns the candidate decay vertex, See Fig. 2.6. It does this by first picking the most energetic cell in layer 2, $L2_1$ (layer 2, 1st photon), as the most probable maximum of energy deposition is found in layer 2, see Fig. 2.4. It then finds the most energetic cell which is within a specific small neighborhood around $L2_1$ in η and ϕ, but in layer 3. This is to ensure it identifies the most energetic cell of the subsequent layer corresponding to the same photon. The specific small neighborhood around $L2_1$ is a square of side $2d_s$ (d_s for 'search distance') centered at $L2_1$. So, $L3_1$ is the most energetic cell of layer 3 whose η and ϕ coordinates are within d_s of $L2_1$'s η and ϕ. Similarly, $L1_1$ and $L0_1$ are found by requiring their η and ϕ coordinates are d_s-close to

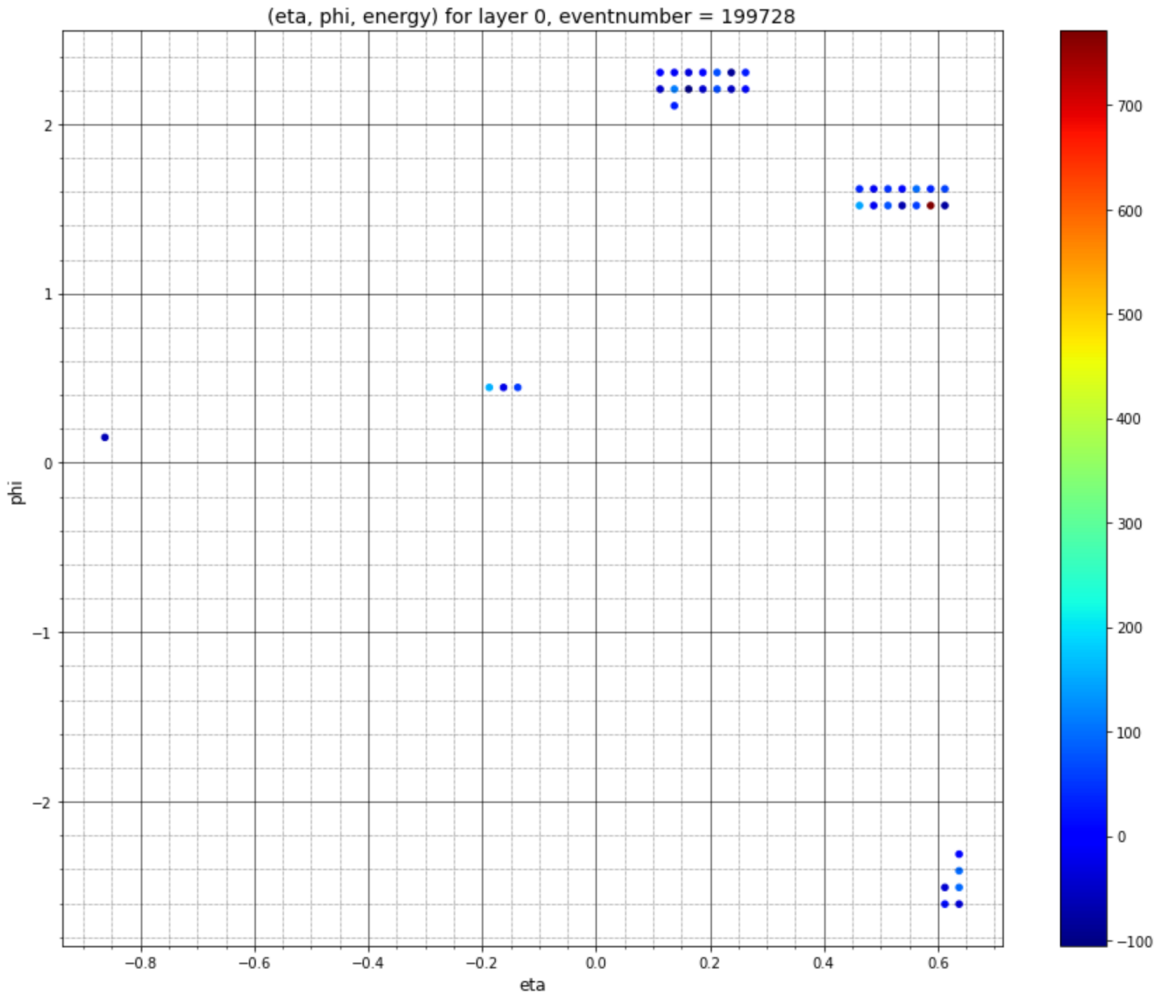

Figure 2.2: Cell-level information for layer 0 of event '199728'. Energy is in MeV.

those of $L2_1$. This way we four cells are obtained, one in each layer, all corresponding to photon 1.

A similar approach is used to find the four cells of the second photon; the same d_s is used and $L2_2$ is the reference cell. But, the difference is in how the most energetic cell of the second photon $L\mu_2$ is identified in a given layer once the first most energetic cell $L\mu_1$ has been found, where $\mu = 0, 1, 2, 3$. To find $L2_2$, say, in order to ensure the algorithm does not choose a cell

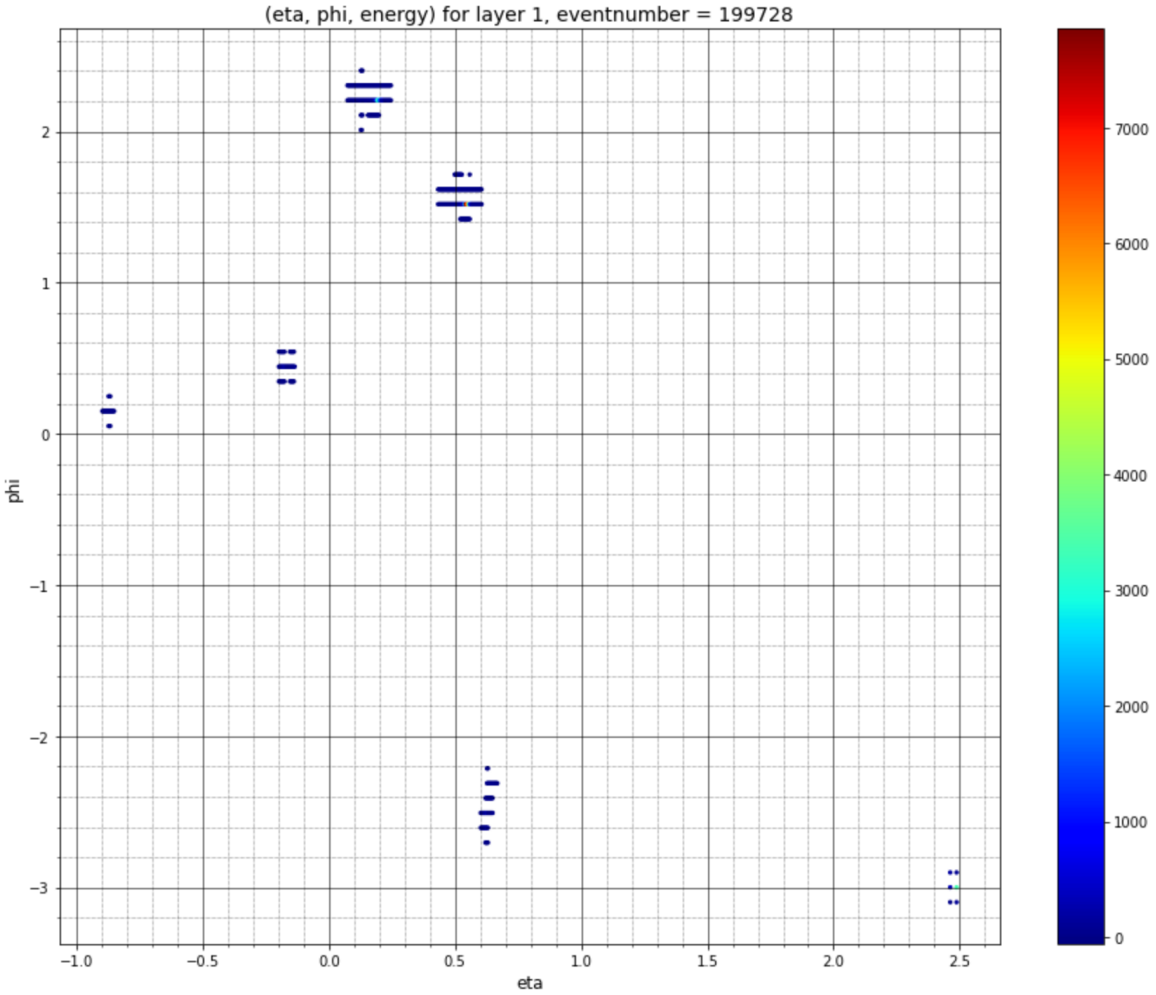

Figure 2.3: Cell-level information for layer 1 of event '199728'. Energy is in MeV.

which actually corresponds to photon 1, it is required to look for the most energetic cell which is *not* within a different specified neighborhood around $L2_1$. This neighborhood would also be a square but with sides $2d_i$ (d_i for 'ignore distance'), centered at $L2_1$. So, $L2_2$ is the most energetic cell in layer 2 that is d_i-away from those of $L2_1$. The remaining cells of photon 2 in the other layers are found in the same way as photon 1's cells, but while making sure these cells are sufficiently far away from the photon 1 cell in

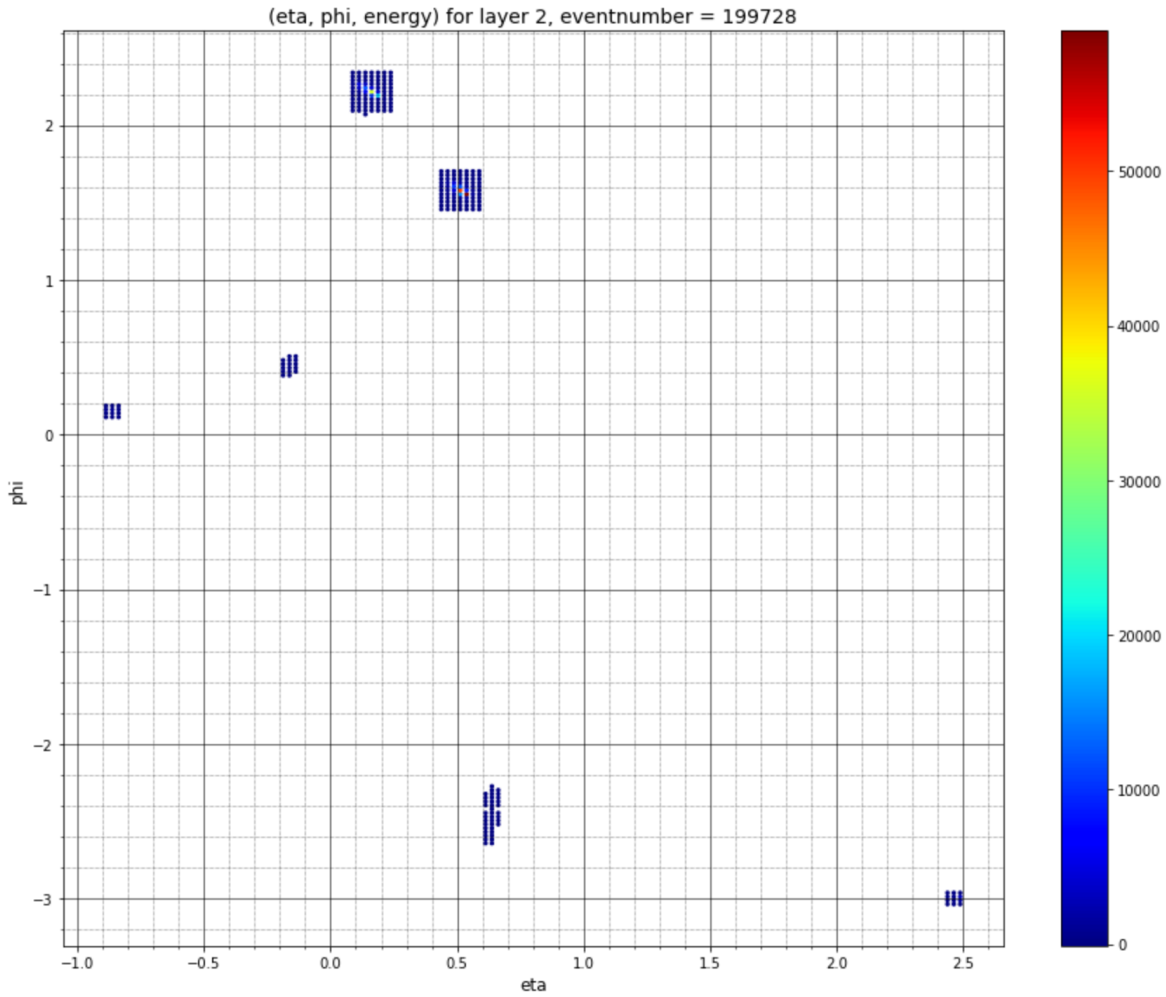

Figure 2.4: Cell-level information for layer 2 of event '199728'. Energy is in MeV. It is easy to identify the two most energetic cells corresponding to the two photons in this layer, and hence this layer was chose as the reference for the algorithm. The choices for d_s and d_i were also informed by the features in layer 2, specifically the size of the cluster.

the respective layer.

Once all cells for each photon in an event have been obtained, a straight line is determined through the 4 cells corresponding to a photon using principal component analysis to obtain that photon's 'track' or trajectory in the

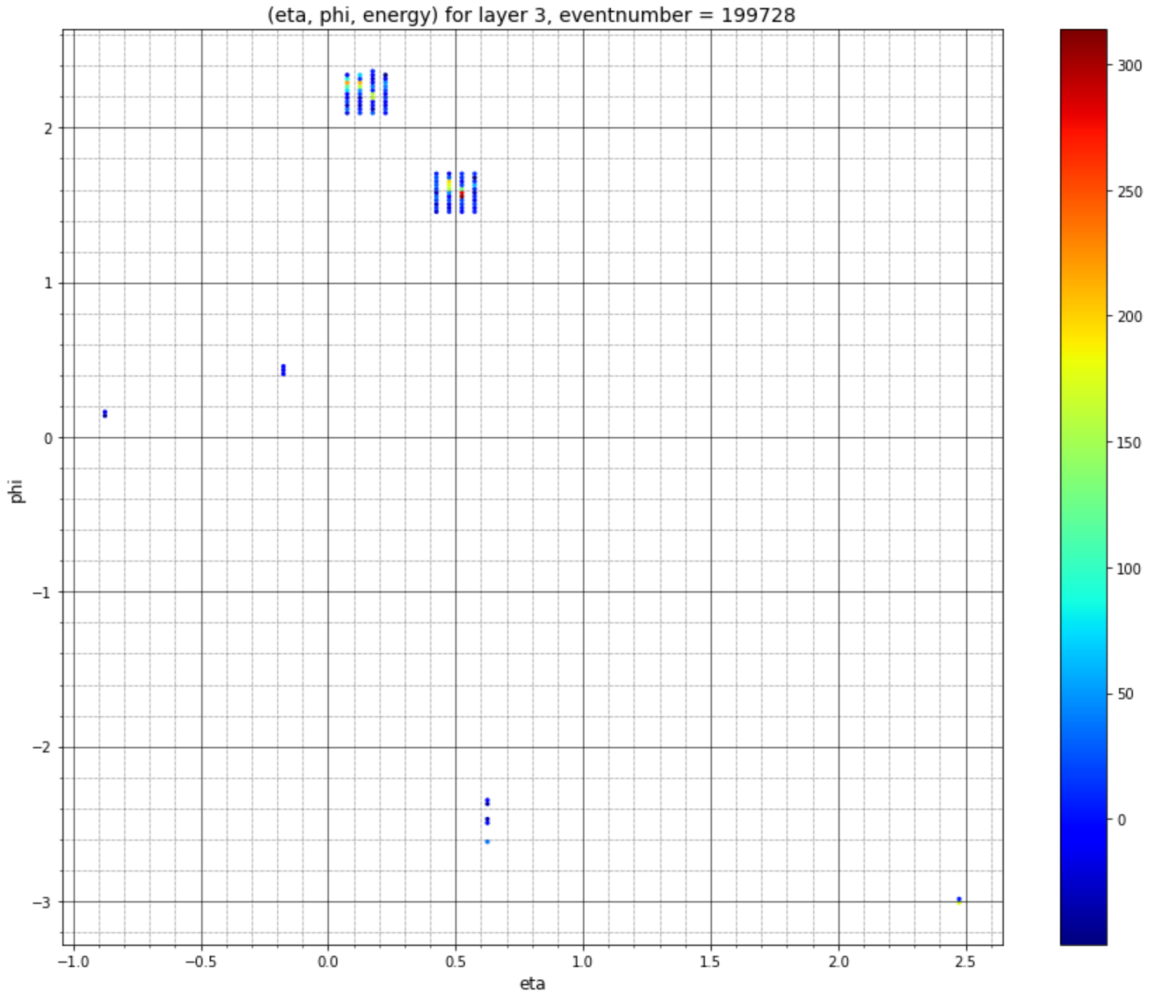

Figure 2.5: Cell-level information for layer 3 of event '199728'. Energy is in MeV.

detector. Since it is highly unlikely that these tracks actually intersect to give us a point due to systematic error, the candidate vertex was found by computing the midpoint of the shortest perpendicular distance connecting the two straight line tracks. The length of this shortest perpendicular distance is a measure of how well the tracks intersect and thus the accuracy of the candidate decay vertex. See Fig. 2.7.

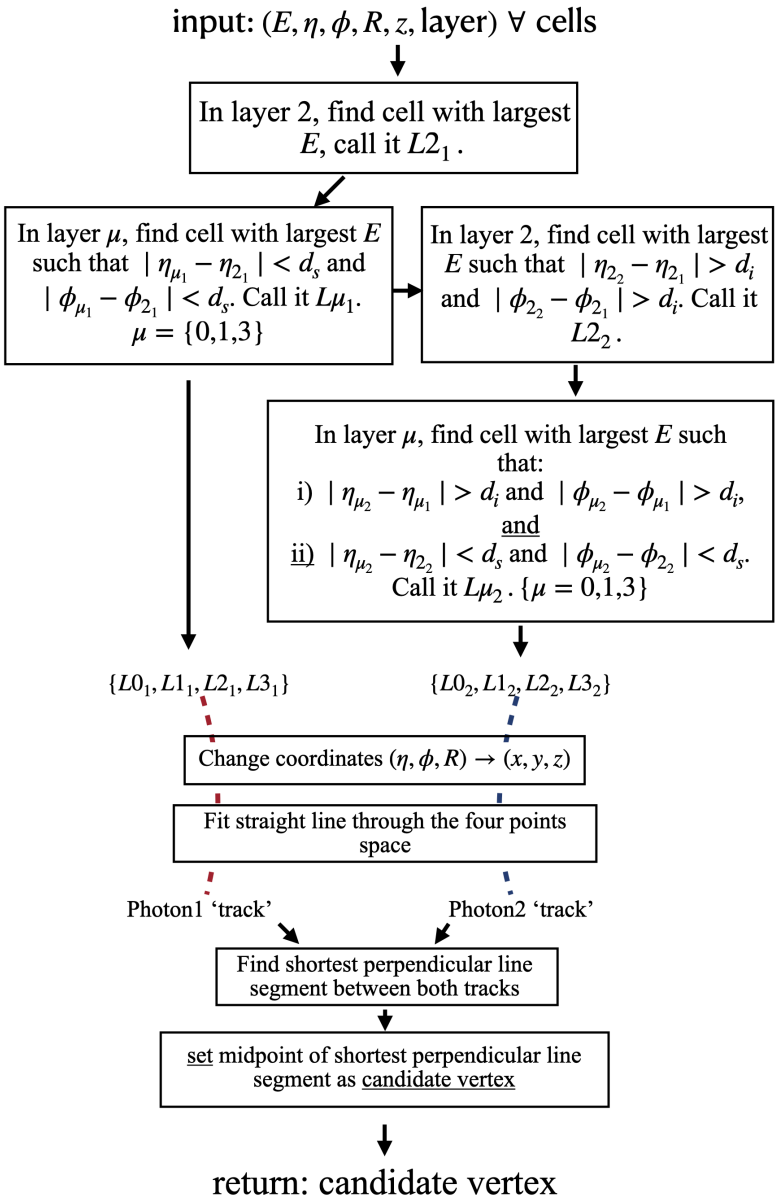

Figure 2.6: Flowchart depicting the algorithm's process.

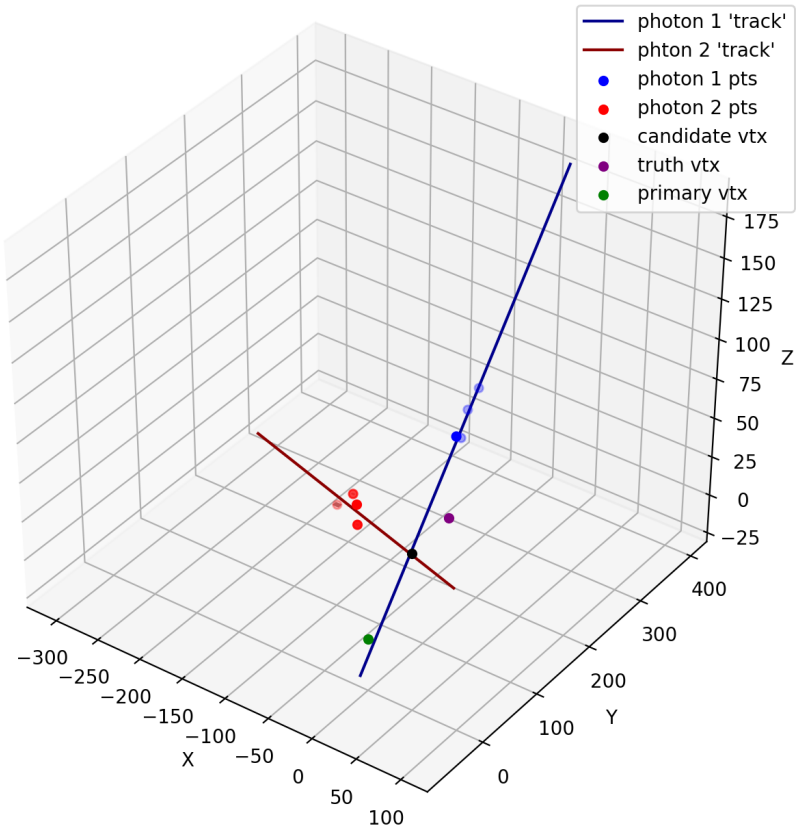

Figure 2.7: Result of the algorithm on event '199728'. All axes are in cm. The shortest perpendicular line segment between the photon tracks is 2.74 cm.

Chapter 3

Results

By the method described above, using $d_s = 0.1$ and $d_i = 0.1$, a candidate vertex was obtained for each event in the master sample. To evaluate whether the candidate vertex is more accurate to the truth vertex in comparison to the primary vertex, the main quantities we look at are the distances between the truth vertex and the candidate vertex, and between the truth vertex and primary vertex. If $d(\text{candidate}, \text{truth}) < d(\text{primary}, \text{truth})$, then the candidate vertex we found is more accurate than the primary vertex. While that by itself does not give us much information about how much more accurate the candidate vertex we found is, the histogram of $d(\text{candidate}, \text{truth})$ and $d(\text{primary}, \text{truth})$ does provide a sense of how the candidate vertex compares. See Fig. 3.1.

.	$d_s = 0.1$	$d_s = 0.125$	$d_s = 0.15$
$d_i = 0.75$	0.535	0.529	0.523
$d_i = 0.1$	0.536	0.530	0.523

Table 3.1: Ratio of number of events with $d(\text{candidate}, \text{truth}) < d(\text{primary}, \text{truth})$ to the total number of events, for different d_s and d_i.

The probability of $d(\text{cand}, \text{truth}) < d(\text{primary}, \text{truth})$ as the distance of the candidate vertex from the origin is varied was also computed. A probability of 0.8 in the 40-45cm bin would mean if the candidate vertex was found to be 40-45cm from the origin, then $d(\text{candidate}, \text{truth}) < d(\text{primary}, \text{truth})$ 80 percent of the time. See Fig. 3.2.

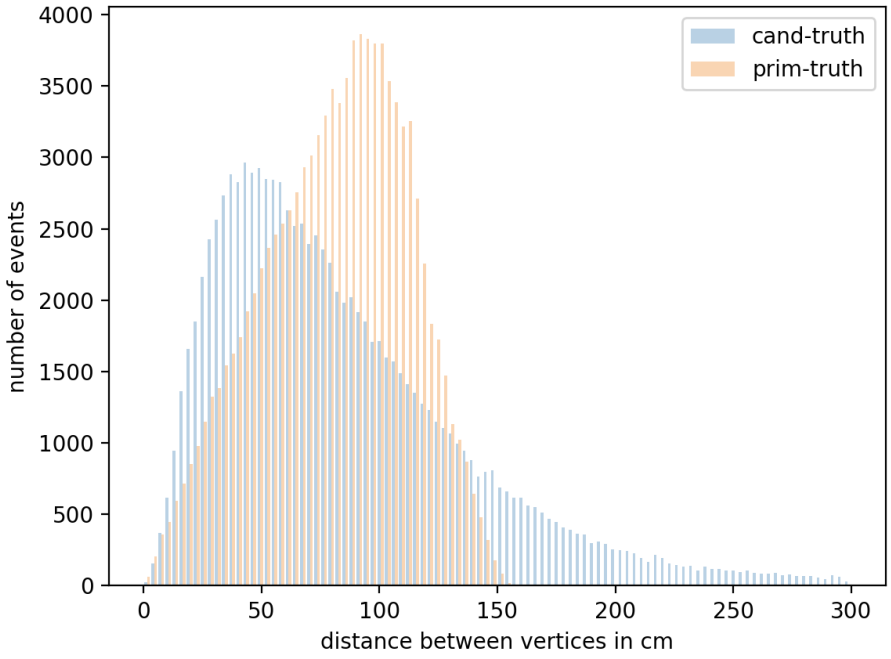

Figure 3.1: Master sample: Distribution of $d(\text{candidate}, \text{truth})$ and $d(\text{primary}, \text{truth})$. Sample size = 101,964.

A collection of sub-samples where events with certain properties was made to investigate whether there are certain regions in the parameter space where the algorithm performs significantly better. Three special selections of the master sample were chosen.

The first sub-sample are the events in which the length of the shortest perpendicular line segment between the photon tracks is less than 10cm. This is a simple selection that can be done to ensure the tracks are 'close' to intersecting (10cm is a rather large window). The closer the tracks are to intersecting, the less ambiguous is the geometric picture of the decay in the detector. We call this sample 1. See Fig. 3.3.

In Sample 2, all the events have candidate vertices within 25cm of the beam pipe (z-axis), see Fig. 3.4. Sample 3 contains the events in which the candidate vertex is in the farther reaches of the the Inner detector, i.e, the candidate vertex is required to either have 50 cm $<|\ z\ |<$ 115 cm, or

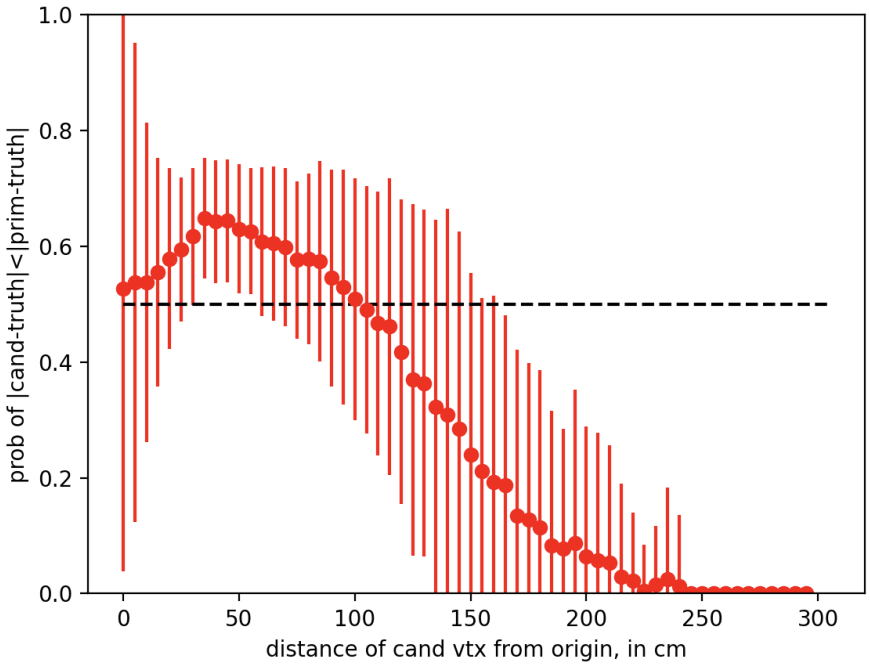

Figure 3.2: Master sample: Probability of $d(\text{cand}, \text{truth}) < d(\text{primary}, \text{truth})$ as a function of the distance between the candidate vertex and the origin. Steps are in 5cm. Dashed line marks 50 percent probability. Sample size = 101,964.

75 cm $<|\ r\ |=$ $\sqrt{x^2+y^2}$ $<$ 100 cm. These are the events with vertices farthest out from the origin, while not crossing into the EM calorimeter. The algorithm was designed for these cases, which should be reconstructed inaccurately by the standard reconstruction. See Fig. 3.5.

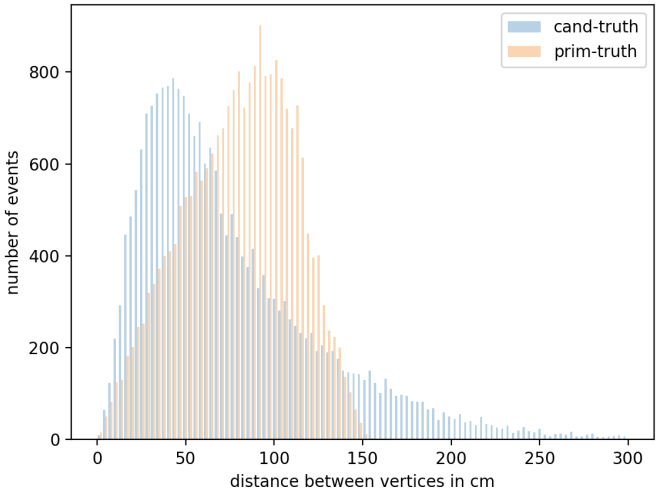

(a) Distribution of $d(\text{candidate}, \text{truth})$ and $d(\text{primary}, \text{truth})$.

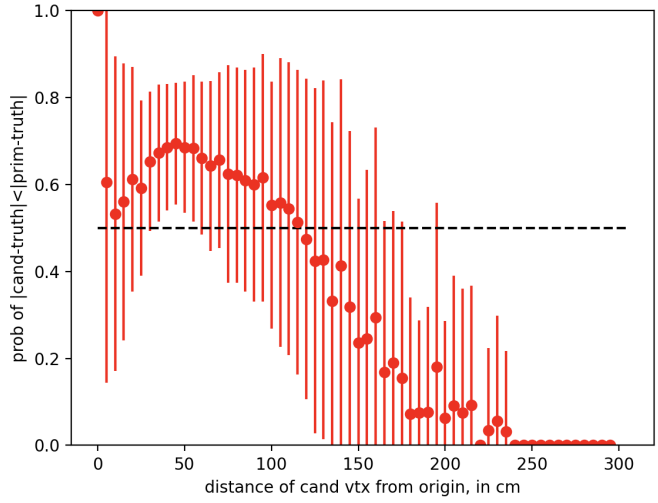

(b) Probability of $d(\text{cand}, \text{truth}) < d(\text{primary}, \text{truth})$ as a function of $d(\text{cand}, \text{truth})$.

Figure 3.3: Sample 1. Length of the shortest perpendicular line segment between the photon tracks is selected to be less than 10 cm. Sample size = 22,808

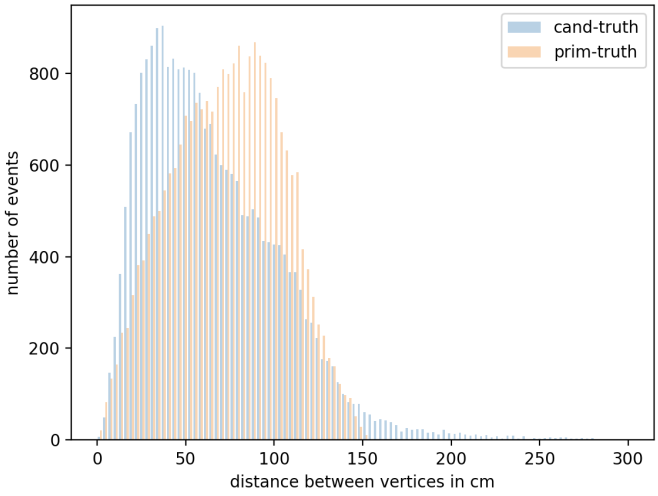

(a) Distribution of $d(\text{candidate}, \text{truth})$ and $d(\text{primary}, \text{truth})$.

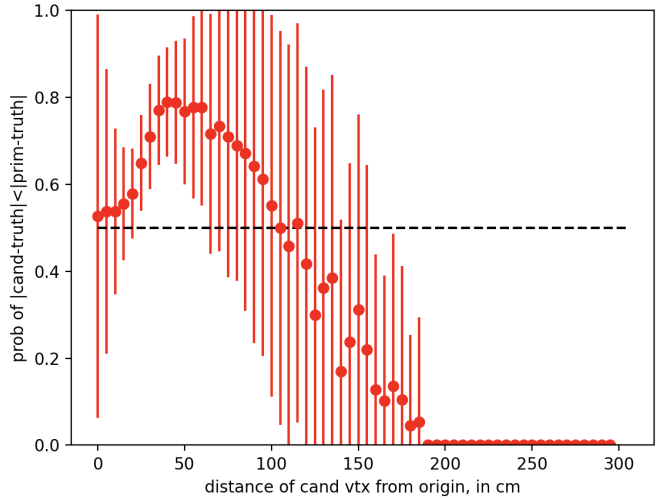

(b) Probability of $d(\text{cand}, \text{truth}) < d(\text{primary}, \text{truth})$ as a function of $d(\text{cand}, \text{truth})$.

Figure 3.4: Sample 2. Candidate vertices within 25cm of the beam pipe (z-axis). Sample size = 24,595

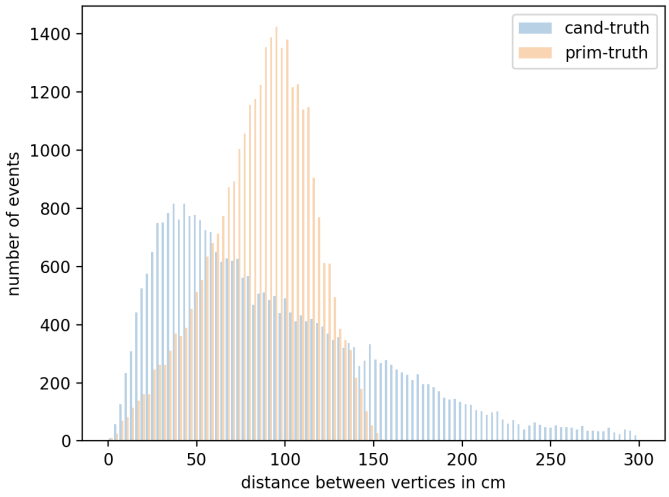

(a) Distribution of $d(\text{candidate}, \text{truth})$ and $d(\text{primary}, \text{truth})$.

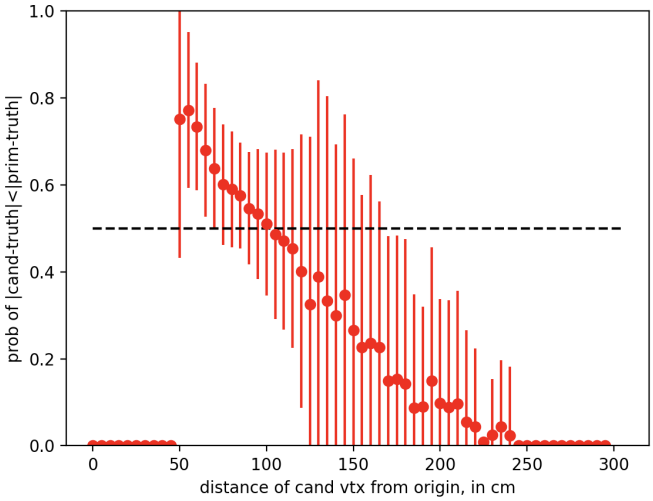

(b) Probability of $d(\text{cand}, \text{truth}) < d(\text{primary}, \text{truth})$ as a function of $d(\text{cand}, \text{truth})$.

Figure 3.5: Sample 3. Candidate vertex has 50 cm $<|\ z\ |<$ 115 cm, or 75 cm $<|\ r\ |= \sqrt{x^2 + y^2} <$ 115 cm. Sample size = 31,312

Chapter 4

Discussion

Several theories points to a few hypothetical particles which might fit the scope of this study, i.e, Higgs-like LLPs that decay into photons with lifetimes less than about 3 ns. Gauge-Mediated SUSY Breaking models include long-lived neutralinos which decays into a gravitino and a photon or Z for a Bino-like or Higgsino-like neutralino, respectively [9]. Even more relevant are an Neutrino models, a class of models that solve the Hierarchy Problem through discrete symmetries that result in colorless top partners that protect the weakscale. In these models long-lived glueballs decay directly into displaced Higgs bosons [10] [12]. Furthermore, as new physics continues to elude the "standard" searches at the LHC, theoretical interest in this area is growing.

The figures for Sample 1 and 2 (Fig. 3.3, 3.4), which represent the events with well-intersecting tracks and vertices near the beam pipe, respectively, are similar to the figures of the master sample (Figs. 3.1, 3.2) in general features. All of them have a peak around 50cm from the origin and tend to fall below 0.5 right after 115cm from the origin, which marks where the EM calorimeter begins. For events in which the candidate vertex was found to be in the EM calorimeter region, the probability of $d(\text{cand}, \text{truth}) < d(\text{primary}, \text{truth})$ is below 0.5 in all the samples. If the decay vertex actually was in the EM region, then the photon may not have information for a particular layer or two, making the reconstruction of the photons less reliable as it would have fewer than four points per photon.

A curious feature in Sample 1 is the supposed probability of 1 of $d(\text{cand}, \text{truth}) < d(\text{primary}, \text{truth})$, when the candidate vertex is within 5 cm of the origin.

This is likely an effect of small number of entries in that particular bin, which can be seen in the size of the error bars. In the case of sample 2, we observe the highest peak in probability. There is an 80 percent chance of $d(\text{cand}, \text{truth}) < d(\text{primary}, \text{truth})$ if the candidate is 50-75cm from the origin and within 25cm from the z axis.

Sample 3 (Fig. 3.5) represents the events where the candidate vertex was found to be farthest from the origin, while not entering the EM calorimeter. Knowing these events, if they occur in actual experiment would be inaccurately reconstructed, it is reassuring to see we see about 80 percent chance of $d(\text{cand}, \text{truth}) < d(\text{primary}, \text{truth})$ around 50 cm from the origin. This value decreases as you move farther away, dropping below 50 percent as you enter the EM calorimeter.

It must be noted that just because $d(\text{candidate}, \text{truth}) < d(\text{primary}, \text{truth})$, it does not mean the candidate vertex is significantly more correct than the primary vertex. The difference could be less than a centimeter and contribute positively to the probability all the same. Nevertheless, a probability greater than fifty percent is a positive result, and if the sample size were to be many orders of magnitude larger (as it would be in actual experiment) we would see many orders more of accurate reconstructions of Higgs-like LLPs with lifetimes less than about 3 ns.

4.1 Further work

The goal would be to develop the algorithm further and use it on real ATLAS data, as it could provide accurate reconstructions of LLPs that decay before the EM calorimeter, and thus can be used in the searches for new physics.

There are several steps to further develop the algorithm. The first is to vary the values of the only parameters that go into the algorithm, d_s and d_i, see Table 3.1. It is possible there is a specific combination we missed that produces better results. This problem suits itself naturally to machine learning techniques, which is an obvious extension of this work.

Another next step would be to cluster together all the cells of a photon. By doing this we could obtain the full energy of the photon (as opposed to those of four cells of a photon). Clustered photons enable us to calculate the invariant mass of the parent particle, the Higgs. Since we know the invariant mass of the Higgs boson (125 GeV), computing the invariant mass

from the sum of the four-vectors of the two photons will serve as another test of accurate reconstruction. In addition, we can use shower shape variables to identify photons better, which will be useful when the layers have higher occupancy.

A possible direction to go towards is to incorporate quantum computing to enhance the algorithm. By use of the Quadratic Unconstrained Binary Optimization (QUBO) [7], a pattern matching technique common in machine learning applications, the process of picking the cells and evaluating how accurate the reconstruction is could become significantly faster, when quantum computing truly takes off.

Lastly, of course, one could investigate different decays. Decays with final state particles such as electrons are good choices as we would not have to go beyond the EM calorimeter and we have physical particle tracks to work with (as opposed to constructing them by fitting a line). To cover a larger set of LLPs, one could look at decays with final state particles as quarks, in which case we would have to extend the algorithm to the Hadronic calorimeter.

4.2 Conclusion

In this study, an algorithm was designed to reconstruct LLP decay vertices using the cell-level information of the EM calorimeter. The algorithm was tested on simulations of events where a Higgs boson was required to decay into two photons at locations far away from the detector. The accuracy of the reconstruction was evaluated by comparing the distance between the candidate and truth decay vertex, and between the primary and truth decay vertex, for all events, and for events in special selections. It was found that the algorithm is most efficient around 50 cm from the origin, i.e, had the highest probability of $d(\text{candidate}, \text{truth}) < d(\text{primary}, \text{truth})$. If the candidate vertex was found 50-75cm from the origin and within 25cm from the z axis, or it was found in the outer regions of the Inner Detector, i.e, the vertex had 50 cm $<|\ z\ |<$ 115 cm, or 75 cm $<|\ r\ |= \sqrt{x^2 + y^2} <$ 115 cm, then there would be an 80 percent chance of $d(\text{candidate}, \text{truth}) < d(\text{primary}, \text{truth})$. This suggests future extensions of the work will be useful in discovering the new physics in the heaps of data discarded by current ATLAS methods.

Bibliography

[1] M. Aaboud, G. Aad, B. Abbott, D. C. Abbott, O. Abdinov, B. Abeloos, D. K. Abhayasinghe, S. H. Abidi, O. S. AbouZeid, and et al. Electron reconstruction and identification in the ATLAS experiment using the 2015 and 2016 LHC proton–proton collision data at $\sqrt{s} = 13$ TeV. *The European Physical Journal C*, 79(8), Aug 2019.

[2] M. Aaboud, G. Aad, B. Abbott, D.C. Abbott, O. Abdinov, B. Abeloos, D.K. Abhayasinghe, S.H. Abidi, O.S. AbouZeid, N.L. Abraham, and et al. Electron and photon energy calibration with the ATLAS detector using 2015–2016 LHC proton-proton collision data. *Journal of Instrumentation*, 14(03):P03017–P03017, Mar 2019.

[3] M. Aaboud, G. Aad, B. Abbott, J. Abdallah, O. Abdinov, B. Abeloos, R. Aben, O. S. AbouZeid, N. L. Abraham, and et al. Reconstruction of primary vertices at the atlas experiment in run 1 proton–proton collisions at the lhc. *The European Physical Journal C*, 77(5), May 2017.

[4] M. Aaboud, G. Aad, B. Abbott, O. Abdinov, B. Abeloos, D. K. Abhayasinghe, S. H. Abidi, O. S. AbouZeid, N. L. Abraham, and et al. Measurement of the photon identification efficiencies with the atlas detector using lhc run 2 data collected in 2015 and 2016. *The European Physical Journal C*, 79(3), Mar 2019.

[5] G. Aad, B. Abbott, J. Abdallah, O. Abdinov, R. Aben, M. Abolins, O. S. AbouZeid, H. Abramowicz, H. Abreu, and et al. Topological cell clustering in the atlas calorimeters and its performance in lhc run 1. *The European Physical Journal C*, 77(7), Jul 2017.

[6] S. Agostinelli, J. Allison, K. Amako, J. Apostolakis, H. Araujo, P. Arce, M. Asai, D. Axen, S. Banerjee, G. Barrand, and et al. Geant4—a simulation toolkit. *Nuclear Instruments and Methods in Physics Research Section A: Accelerators, Spectrometers, Detectors and Associated Equipment*, 506(3):250–303, Jul 2003.

[7] Endre Boros, Peter L. Hammer, and Gabriel Tavares. Local search heuristics for quadratic unconstrained binary optimization (qubo). *Journal of Heuristics*, 13(2):99–132, April 2007.

[8] Rene Brun and Fons Rademakers. Root — an object oriented data analysis framework. *Nuclear Instruments and Methods in Physics Research Section A: Accelerators, Spectrometers, Detectors and Associated Equipment*, 389(1):81 – 86, 1997. New Computing Techniques in Physics Research V.

[9] Nathaniel Craig, Andrey Katz, Matt Strassler, and Raman Sundrum. Naturalness in the dark at the lhc. *JHEP*, 07:105, 2015.

[10] Jose E. Juknevich. Pure-glue hidden valleys through the higgs portal. *JHEP*, 08:121, 2010.

[11] David J. Lange. The evtgen particle decay simulation package. *Nuclear Instruments and Methods in Physics Research Section A: Accelerators, Spectrometers, Detectors and Associated Equipment*, 462(1):152 – 155, 2001. BEAUTY2000, Proceedings of the 7th Int. Conf. on B-Physics at Hadron Machines.

[12] Lawrence Lee, Christian Ohm, Abner Soffer, and Tien-Tien Yu. Collider searches for long-lived particles beyond the standard model. *Progress in Particle and Nuclear Physics*, 106:210–255, May 2019.

[13] Torbjörn Sjöstrand, Stefan Ask, Jesper R. Christiansen, Richard Corke, Nishita Desai, Philip Ilten, Stephen Mrenna, Stefan Prestel, Christine O. Rasmussen, and Peter Z. Skands. An introduction to pythia 8.2. *Computer Physics Communications*, 191:159–177, Jun 2015.

[14] S. Stärz. Upgraded readout electronics for the atlas lar calorimeter at the phase i of lhc. *Nuclear Instruments and Methods in Physics Re-*

search Section A: Accelerators, Spectrometers, Detectors and Associated Equipment, 718:115–117, Aug 2013.